BJR

Received:
9 September 2014

Revised:
24 December 2014

Accepted:
22 January 2015

doi: 10.1259/bjr.20140601

Cite this article as:
Reichert M, Ai T, Morelli JN, Nittka M, Attenberger U, Runge VM. Metal artefact reduction in MRI at both 1.5 and 3.0 T using slice encoding for metal artefact correction and view angle tilting. Br J Radiol 2015;88:20140601.

FULL PAPER

Metal artefact reduction in MRI at both 1.5 and 3.0 T using slice encoding for metal artefact correction and view angle tilting

[1]M REICHERT, MD, [2]T AI, MD, PhD, [3]J N MORELLI, MD, [4]M NITTKA, PhD, [1]U ATTENBERGER, MD and [5]V M RUNGE, MD

[1]Department of Clinical Radiology and Nuclear Medicine, University Medical Center Mannheim, Medical Faculty Mannheim, Heidelberg University, Manheim, Germany
[2]Department of Radiology, Tongji Hospital, Tongji Medical College, Huazhong University of Science and Technology, Wuhan, Hubei, China
[3]Russell H. Morgan Department of Radiology and Radiological Science, Johns Hopkins University School of Medicine, Baltimore, MD, USA
[4]Siemens Healthcare Sector, Application Development, Erlangen, Germany
[5]Institute for Diagnostic and Interventional Radiology, University Hospital Zurich, Zurich, Switzerland

Address correspondence to: Dr Tao Ai
E-mail: *aitao007@hotmail.com*

Objective: To compare metal artefact reduction in MRI at both 3.0 T and 1.5 T using different sequence strategies.
Methods: Metal implants of stainless steel screw and plate within agarose phantoms and tissue specimens as well as three patients with implants were imaged at both 1.5 T and 3.0 T, using view angle tilting (VAT), slice encoding for metal artefact correction with VAT (SEMAC-VAT) and conventional sequence. Artefact reduction in agarose phantoms was quantitatively assessed by artefact volume measurements. Blinded reads were conducted in tissue specimen and human imaging, with respect to artefact size, distortion, blurring and overall image quality. Wilcoxon and Friedman tests for multiple comparisons and intraclass correlation coefficient (ICC) for interobserver agreement were performed with a significant level of $p < 0.05$.
Results: Compared with conventional sequences, SEMAC-VAT significantly reduced metal artefacts by 83% ± 9% for the screw and 89% ± 3% for the plate at 1.5 T; 72% ± 7% for the screw and 38% ± 13% for the plate at 3.0 T ($p < 0.05$). In qualitative analysis, SEMAC-VAT allowed for better visualization of tissue structures adjacent to the implants and produced better overall image quality with good interobserver agreement for both tissue specimen and human imaging (ICC = 0.80–0.99; $p < 0.001$). In addition, VAT also markedly reduced metal artefacts compared with conventional sequence, but was inferior to SEMAC-VAT.
Conclusion: SEMAC-VAT and VAT techniques effectively reduce artefacts from metal implants relative to conventional imaging at both 1.5 T and 3.0 T.
Advances in knowledge: The feasibility of metal artefact reduction with SEMAC-VAT was demonstrated at 3.0-T MR. SEMAC-VAT significantly reduced metal artefacts at both 1.5 and 3.0 T. SEMAC-VAT allowed for better visualization of the tissue structures adjacent to the metal implants. SEMAC-VAT produced consistently better image quality in both tissue specimen and human imaging.

Orthopaedic implants are commonly and increasingly used in patients with traumatic injuries and musculoskeletal tumours. The imaging evaluation of post-surgical complications, including mainly periprosthetic osteolysis, loosening, malpositioning, instability and infection, is strongly demanded in the clinical scenario. In this context, MRI is supposed to be the imaging modality of choice for such applications because it has superior soft-tissue contrast.[1–3] However, the diagnostic accuracy and efficiency of MRI has been compromised by the susceptibility artefacts caused by metal implants.[4,5]

Briefly, susceptibility artefacts result from local inhomogeneity of the main magnetic field, which will cause spin dephasing and frequency shifting of the tissue structures surrounding the metal implants. Intravoxel dephasing decreases the signal received and results in hypointense areas on the MR images. Frequency shifting results in spatial misregistration seen as bright and dark areas on the image as well as geometric distortion of surrounding anatomies.[6,7] In such cases, spin echo (SE) or turbo SE (TSE) sequences are less sensitive to the susceptibility effects and are preferred during MRI of metal implants

owing to the application of a 180° refocusing pulse. An increased radiofrequency (RF) bandwidth, a higher readout bandwidth, a smaller slice thickness, shorter echo spacing and choosing short tau inversion recovery (STIR) for fat suppression instead of spectral fat saturation are also essential approaches for metal artefact correction to various degrees.[8]

Based on the knowledge above, several specific sequence strategies have been recently developed for more effective reduction of metal-induced artefacts, including view angle tilting (VAT), slice encoding for metal artefact correction with VAT technique (SEMAC-VAT) and multiacquisition with variable resonance image combination (MAVRIC).[9–12] VAT technique uses an extra gradient in the slice-select direction during the readout gradient, such that the image pixels appear as if they were viewed from an angle. The sum of artefactual frequency shifts in the slice-select and the readout direction results in a frequency shift in the oblique direction. By viewing from this oblique angle during readout, the received signal can be projected onto the corrected pixel position of the image matrix. In this way, in-plane artefacts of metal implants can be corrected at the cost of image blurring.[13] SEMAC technique involves additional phase-encoding steps (z-encoding gradient) into the slice direction in order to resolve geometric distortion along the slice profile. During image reconstruction, this information is used to sort distorted pixels into their correct slice positions, thus through-plane distortion can be corrected. The principal drawbacks of this technique are the requisite increase in scan time and specific absorption rate (SAR). Thereafter, SEMAC has been incorporated with VAT and named as SEMAC-VAT, which allows for better correction of both in-plane and through-plane artefacts of metal implants.[14] MAVRIC technique is based on a three-dimensional fast spin echo sequence, by applying multiple spectral excitations to recover off-resonance signals caused by metal implants. In addition, a hybrid method of MAVRIC and SEMAC was also proposed to enhance the correction of through-plane distortion by adding a z-encoding gradient into MAVRIC spectral acquisitions.[15]

From our previous study, SEMAC-VAT techniques have been proven to be the superior method for artefact reduction of different metal implants at 1.5 T. However, the efficacy and efficiency of those advanced imaging techniques at 3.0 T systems have not been investigated yet. In this study, we are trying to evaluate the efficacy and efficiency of VAT and SEMAC-VAT in metal artefact reduction of MRI at both 3.0 and 1.5 T, in the presence of orthopaedic implants.

METHODS AND MATERIALS

Imaging technique

A work-in-progress software package ("WARP" WIP#648; Siemens Healthcare, Erlangen, Germany) was utilized for MRI. The WIP was optimized with two-dimensional TSE sequence including VAT and SEMAC techniques featured with increased RF pulse bandwidth. The SEMAC technique was integrated with the VAT technique in this package. SEMAC can be switched on and off independently as was carried out in this study. In all cases described below, the metal hardware was oriented parallel to the direction of the main magnetic field ($B0$). The experimental design is detailed in Table 1.

Phantom imaging

A stainless steel screw (Smith & Nephew 3.5-mm standard and cortical 38-mm locking screws) and a stainless steel plate (Smith & Nephew Periloc 6-hole 4.5-mm locking plates) were placed in two separate plastic containers filled with agarose gel. Each implant was placed in the central aspect of each phantom. Each phantom was positioned at the centre of a flexible four-element receiver coil and scanned on both 1.5 T (Magnetom® Espree; Siemens Healthcare) and 3.0 T (Magnetom Verio) MR systems. Images with T_1 weighted (T_1), T_2 weighted (T_2), proton density-weighted (PD) and STIR contrast were obtained with three different techniques, including the conventional sequence (called product), VAT and SEMAC-VAT, respectively (resulting in 12 scans for each phantom). The details of MR parameters are listed in Table 2. In this study, a RF bandwidth of 1.8 kHz was chosen for SEMAC-VAT. Combined with parallel imaging [generalized autocalibrating partially parallel acquistions (GRAPPA), acceleration factor of two], which was used in all sequences, the scan time was shortened compared with acquisitions without GRAPPA.

Scan time was considerably reduced by utilizing dedicated acquisition techniques such as parallel imaging, partial Fourier sampling and long echo trains. Turbo factors were held constant

Table 1. Experimental design with sequence techniques and image contrasts

Sequences	Agarose phantom	Tissue specimen	Human
View angle tilting	Coronal T_1, T_2, PD, STIR	Coronal T_1, T_2, PD, STIR	None
	Axial, sagittal T_1 and PD		
Slice encoding for metal artefact correction	Coronal T_1, T_2, PD, STIR	Coronal T_1, T_2, PD, STIR	Coronal STIR
	Axial, sagittal T_1 and PD		Axial T_1
			Sagittal PD
Product	Coronal T_1, T_2, PD, STIR	Coronal T_1, T_2, PD, STIR	Coronal STIR
	Axial, sagittal T_1 and PD		Axial T_1
			Sagittal PD

PD, proton density-weighted imaging; Product, conventional sequence; STIR, short tau inversion recovery; T_1, T_1 weighted imaging; T_2, T_2 weighted imaging.

Table 2. Imaging parameters at both 1.5 and 3.0 T

Imaging parameters		Product				VAT				SEMAC-VAT			
		T_1	T_2	PD	STIR	T_1	T_2	PD	STIR	T_1	T_2	PD	STIR
Repetition time/echo time (ms) (1.5 T *vs* 3.0 T)		650/16	5000/71	3000/31	3500/35	650/16	6000/71	3000/28	3500/35	650/16	6000/77	3500/34	3500/35
		886/7	5010/77	3610/35	3500/42	885/14	5010/77	3610/35	3500/42	886/7	5010/77	3610/35	6290/42
Readout bandwidth		781 Hz per pixel for product				930 Hz per pixel for VAT				930 Hz per pixel for SEMAC-VAT			
Field of view		180 × 180 mm for all											
Matrix		256 × 256 for all											
Slice		2.5 mm for all											

PD, proton density-weighted imaging; Product, conventional sequence; SEMAC, slice encoding for metal artefact correction; STIR, short tau inversion recovery; T_1, T_1 weighted imaging; T_2, T_2 weighted imaging; VAT, view angle tilting.

at one for both 1.5 and 3.0 T imaging. Scan times at 3.0 T were prolonged relative to 1.5 T owing to adjustments to repetition time and echo time, which were made for imaging at that field strength. Additionally, imaging at 3.0 T was prolonged by increased time utilized for shimming. Thus, the scan time at 1.5 T was about 2–3 min for the conventional and VAT sequences and 7–12 min for the SEMAC-VAT sequences with 15 steps. The scan time at 3.0 T was 3–4 min for the conventional and VAT sequences and 8–13 min for the SEMAC-VAT sequences with 15 steps.

Artefact volume owing to metal implant was measured offline using a dedicated workstation (GE Advantage Workstation AW4.2; GE Healthcare, Waukesha, MI). The semi-quantitative approach for artefact volume quantification originally described in Lee et al[16] was adopted for analysis of each pulse sequence. This method is favourable owing to its ease of implementation and ability to account for both high and low signal intensity artefacts. To summarize the approach, an agarose gel phantom without any metal implants was first imaged. The signal intensity distribution in the standardized central area was calculated utilizing the histogram tool in the workstation. For clarity, the calculated values are mean, 468 and standard deviation (SD), 32.8. In this case, the normal range of signal intensities was defined as being voxels with signal intensity within three SDs of the mean signal intensity (*i.e.* 369–566).

The agarose gel containing the metal implant was imaged with the same pulse sequence. A histogram analysis of signal intensity was similarly performed by drawing a region of interest encompassing the agarose gel. The number of pixels falling outside the normal range of signal intensities was computed, and these were considered artefacts. In reality, this measurement reflects both artefactual signal and true signal void from the actual metal hardware. Thus, if a MR sequence could theoretically be performed without any associated artefacts, the value of this measurement would still be greater than that of the blank agarose phantom, as the signal void associated with the actual metal implant would still be included in the measurement. However, signal void corresponding to the actual metal hardware is present in every case, and thus relative comparisons of artefacts can still reliably be made among sequences. To calculate a total volume of artefacts, analogous calculations were performed throughout the entire imaging volume. The method described is illustrated in part in Figure 1.

Tissue specimen imaging

The animal cadaver study was conducted in compliance with all ethical standards at our institution. A stainless steel plate was surgically attached to the femur of a pig, with six stainless steel screws. The pig legs were imaged first on a 1.5-T MR system (Magnetom Espree, Siemens) and subsequently on a 3.0-T MR system (Magnetom Verio, Siemens). The standard four-channel flex coils were used for image acquisitions at both field strengths. Imaging parameters were held as constant as possible for the different field strengths, including field of view = 18 cm; image matrix = 256 × 256; and slice thickness = 2.5 mm. Imaging was performed in the coronal plane. T_1, T_2, PD and STIR image contrasts were acquired with all three specific techniques including product, VAT and SEMAC-VAT.

Figure 1. Schematic illustration of the volumetric measurement of metal artefacts. MR image of blank agarose phantom (a) with associated histogram analysis (b) was performed within the volume of interest. Mean signal intensity (SI) was 468.0 with standard deviation (SD) of 32.8. The normal range of SI was then defined as mean ± 3 SDs for pure agarose gel at the same concentration. When the normal range was applied into the corresponding MR image of the phantom with metallic implant (c) and associated SI histogram (d), all the pixels with SI outside the normal range (lower threshold = 369 and upper threshold = 566) were considered as metal-induced artefacts. The measurement was completed throughout the entire image volume for volumetric calculation of metal artefacts.

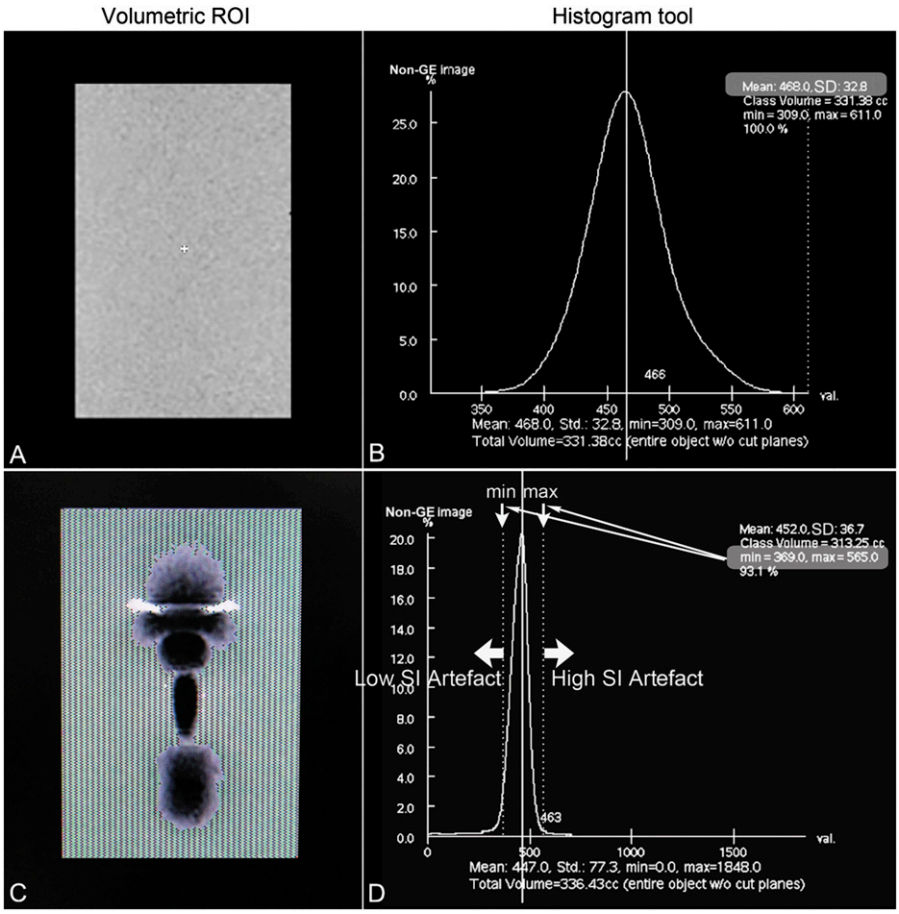

The images from the tissue phantom were assessed by a blinded read. Three readers with more than 5 years' experience in diagnostic radiology evaluated the images. The readers were not aware of the magnetic field strength or sequence type at the time of interpretation. Images with two different sequences and two different field strengths were evaluated on the basis of the following aspects: (1) size of the metal artefact, (2) structure distortion adjacent to the metal, (3) image blurring, (4) visualization ability of the bone marrow, bone cortex and soft tissue, as well as (5) overall image quality. The images were graded by using a four-point scale (Table 3). The images from each technique with the same contrast were compared side by side, with the direct comparison of the results from two different field strengths.

Patient imaging

The human study was approved by the institutional review board at our university hospital. The principles of the Declaration of Helsinki and its subsequent amendments were followed. After informed consent was obtained, three patients (1 male; 2 females; age range, 48–58 years) with metal implants were included to provide *in vivo* assessments. All patients had undergone surgical fixation with metal implants from a few months to several years prior to this study. Evaluated implants included stainless steel, titanium alloy and cobalt chromium. All examinations were performed on both the 1.5 and 3.0 T Siemens scanners. A 4-channel flex coil, 15-channel knee coil and 16-channel foot/ankle coil were specifically used for different study subjects. STIR coronal, T_1 axial, PD sagittal images were acquired with the conventional sequence and SEMAC-VAT technique. The overall performance of artefact reduction was also qualitatively assessed by a blinded read by the three readers, referring to the scoring criteria described above.

STATISTICAL ANALYSIS

Statistical analysis was performed using the commercial statistical software SPSS® v. 18 (SPSS Inc., Chicago, IL). The results were presented with mean ± SD. Non-parametric Wilcoxon and Friedman tests were used for the statistical comparison among different imaging protocols. As evaluated by multiple readers, intraclass correlation coefficient (ICC) was used to calculate the

Table 3. Qualitative evaluation of tissue specimen imaging with a four-point scale scoring system

Evaluation indicators	Scoring criteria (four-point scale)			
	1	2	3	4
Artefact size	Small amount of artefact	Median amount of artefact	Large amount of artefact	Extensive artefact
Structure distortion adjacent to the metal	Slight distortion	Moderate distortion	Severe distortion	Extensive distortion
Image blurring	No blurring	Barely perceivable blurring	Slight blurring	Moderate blurring
Visualization of the bone marrow, cortex and soft tissues	Good visualization	Moderate visualization	Poor visualization	Very poor visualization
Overall image quality	Very good image quality; high diagnostic performance	Good image quality; medium diagnostic performance	Acceptable image quality; low diagnostic performance	Poor image quality; poor diagnostic performance

The images with the conventional (product) and slice encoding for metal artefact correction with view angle tilting sequence technique between 1.5 and 3.0 T were assessed by three readers in blinded reads for metal artefact reduction.

interobserver agreement. The agreement was explained as follows: ICC <0.40 indicated poor agreement, $0.40 \leq \text{ICC} < 0.80$ indicated medium agreement and ICC ≥ 0.80 indicated good agreement among the scoring of the three readers. A $p < 0.05$ was considered statistically significant.

RESULTS

When comparing with the conventional sequence (named as product in the tables and figures), the average metal artefact volume was dramatically reduced by the VAT and SEMAC-VAT at both 1.5 and 3.0 T (Figures 2 and 3). For the stainless steel screw, the average metal artefact volume was reduced by 65% ± 10% with VAT and 83% ± 9% with SEMAC-VAT at 1.5 T, and 45% ± 15% with VAT and 72% ± 7% with SEMAC-VAT at 3 T. For the stainless steel plate, the average metal artefact volume was reduced by 71% ± 7% with VAT and 89% ± 3% with SEMAC-VAT at 1.5 T and by 19% ± 11% with VAT and 38% ± 13% with SEMAC-VAT at 3.0 T (Table 4). Statistical differences were found for all the comparisons when applying the Friedman test ($\chi^2 = 8.0$; $p < 0.05$). A similar trend of artefact reduction was also found on the different image contrasts for each metal implant and magnetic field (Figure 4).

When compared with 1.5 T, the average artefact volume at 3.0 T was increased by 104% ± 65% with product sequence, 360% ± 212% with VAT and 670% ± 422% with SEMAC-VAT based on the four image contrasts and both metal implants. However, the SEMAC-VAT at 3.0 T had almost the same amount of the metal artefact compared with the product sequence at 1.5 T on the corresponding image contrasts (Wilcoxon test, $Z = -0.420$; $p = 0.674$).

Figure 2. Agarose phantom containing one stainless steel screw evaluated at 1.5 T (a, b) and 3.0 T (c, d) with T_1 weighted conventional sequence (a, c) and slice encoding for metal artefact correction with view angle tilting technique (b, d). At both field strengths, a substantial reduction in metal artefact was noted, although overall the artefact was greater at 3.0 T.

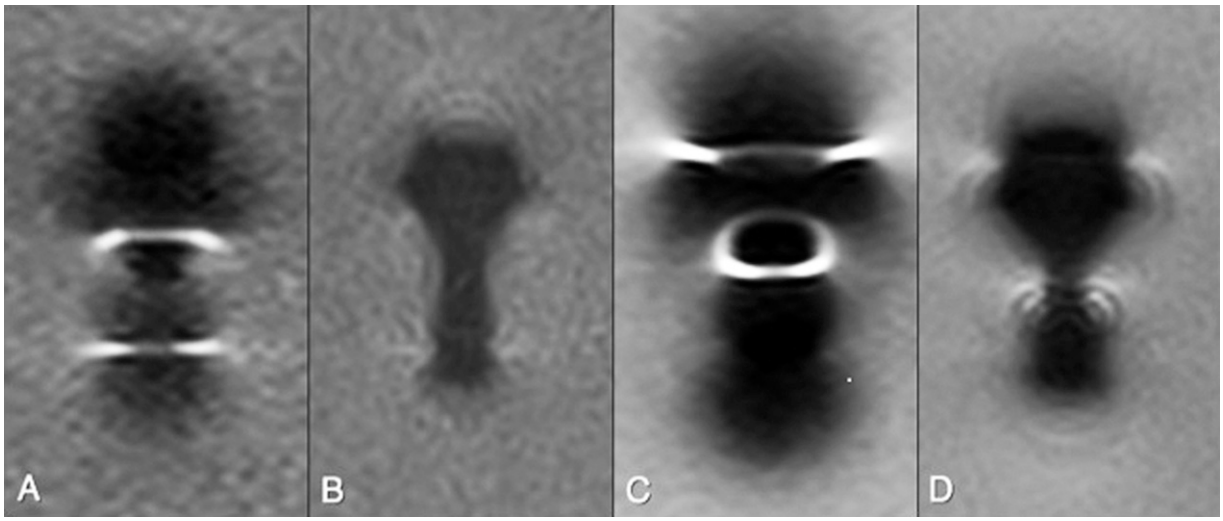

Figure 3. Agarose phantom containing one stainless steel plate evaluated at 3.0 and 1.5 T with proton density-weighted conventional sequence, view angle tilting (VAT) and slice encoding for metal artefact correction (SEMAC)-VAT technique. A minor reduction in metal artefact was noted on VAT images, and a substantial reduction in metal artefact was demonstrated on SEMAC-VAT images on both magnetic fields. Product, conventional sequence.

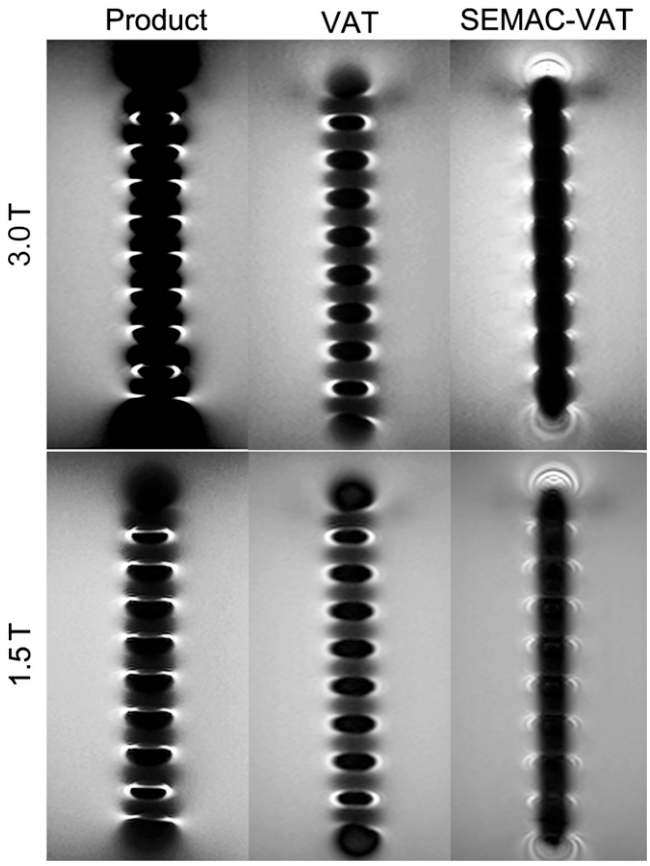

SEMAC-VAT significantly corrected the metal artefact in tissue specimen imaging at both 1.5 and 3.0 T (Figure 5). In the qualitative analysis of tissue specimen imaging, the mean scores of artefact size from the three readers were 3.00 ± 0.58 for product at 1.5 T, 1.08 ± 0.28 for SEMAC-VAT at 1.5 T, 3.83 ± 0.37 for product at 3.0 T and 2.08 ± 0.49 for SEMAC-VAT at 3.0 T (Friedman test, $\chi^2 = 30.3$). The mean scores of structure distortion were 3.25 ± 0.43 for product at 1.5 T, 1.17 ± 0.37 for SEMAC-VAT at 1.5 T, 3.75 ± 0.43 for product at 3.0 T and 1.83 ± 0.37 for SEMAC-VAT at 3.0 T (Friedman test, $\chi^2 = 31.3$). The mean scores of image blurring were 2.33 ± 0.75 for product at 1.5 T, 3.75 ± 0.43 for SEMAC-VAT at 1.5 T, 1.08 ± 0.28 for product at 3.0 T and 2.83 ± 0.69 for SEMAC-VAT at 3.0 T (Friedman test, $\chi^2 = 26.7$). The mean scores of visualization ability to the bone marrow, cortex and soft tissues were 3.17 ± 0.80 for product at 1.5 T, 1.17 ± 0.37 for SEMAC-VAT at 1.5 T, 3.58 ± 0.49 for product at 3.0 T and 2.08 ± 0.64 for SEMAC-VAT at 3.0 T (Friedman test, $\chi^2 = 25.7$). The mean scores of overall image quality were 3.42 ± 0.86 for product at 1.5 T, 1.42 ± 0.49 for SEMAC-VAT at 1.5 T, 3.50 ± 0.50 for product at 3.0 T and 1.83 ± 0.80 for SEMAC-VAT at 3.0 T (Friedman test, $\chi^2 = 23.1$). There were statistically significant differences for all the comparisons above ($p < 0.001$), with good agreements among the three readers (ICC = 0.80–0.99; $p < 0.001$; Table 5).

For the imaging of the patients with different metal implants, SEMAC-VAT technique markedly reduced the metal artefact in MRI at both 1.5 and 3.0 T (Figure 6). With qualitative evaluation by the three readers, the overall performance of artefact reduction was ranked from the best to the worst by SEMAC-VAT at 1.5 T > SEMAC-VAT at 3.0 T > product at 1.5 T > product at 3.0 T for T_1 and PD images. For STIR, however, it was ranked by SEMAC-VAT at 3.0 T > SEMAC-VAT at 1.5 T > product at 1.5 T > product at 3.0 T. There was good agreement among the three readers in the ranking of human scans [ICC = 0.940 (0.874–0.975); $p < 0.001$].

DISCUSSION

The clinical use of 3.0-T MR systems continues to increase principally owing to the improved signal-to-noise ratio (SNR) relative to 1.5 T, which can be traded for either higher spatial resolutions and/or shorter scan times. Depending on the strength of the main magnetic field and magnetic susceptibility of the implanted metal hardware, however, substantial changes of the local field around the implant may occur. As a consequence, MRI of the structures adjacent to metal implants suffers from severe signal off-resonance and dephasing effects. In this case, the increased susceptibility artefacts at 3.0 T prevents its mainstream use for imaging of patients with prosthetic implants,[17] whereas 1.5 T MR system has been considered clinically useful for evaluating periprosthetic tissue.[18,19]

Table 4. Measured artefact volume (cm^3) and the according percentage of artefact reduction for each evaluated sequence compared with conventional acquisition based on four image contrasts

Magnetic field	Metallic implant	Product	VAT	Slice encoding for metal artefact correction-VAT
1.5 T	SS screw	29.3 ± 18.8	9.9 ± 6.4 (65% ± 10%)	3.8 ± 0.8 (83% ± 9%)
	SS plate	279.6 ± 75.9	80.4 ± 24.6 (71% ± 7%)	30.8 ± 9.7 (89% ± 3%)
3.0 T	SS screw	57.5 ± 23.2	30.0 ± 10.1 (45% ± 15%)	17.0 ± 10.9 (72% ± 7%)
	SS plate	480.4 ± 49.2	394.4 ± 76.9 (19% ± 11%)	304.4 ± 87.9 (38% ± 13%)

Product, conventional sequence; SS, stainless steel; VAT, view angle tilting.
The results are expressed as mean ± standard deviation.

Figure 4. Metal artefact reduction in volume for both metal implants [stainless steel (SS) screw and plate] in different image contrasts at both 1.5 and 3.0 T. PDWI, proton density-weighted imaging; SEMAC, slice encoding for metal artefact correction; STIR, short tau inversion recovery; T1WI, T_1 weighted imaging; T2WI, T_2 weighted imaging; VAT, view angle tilting.

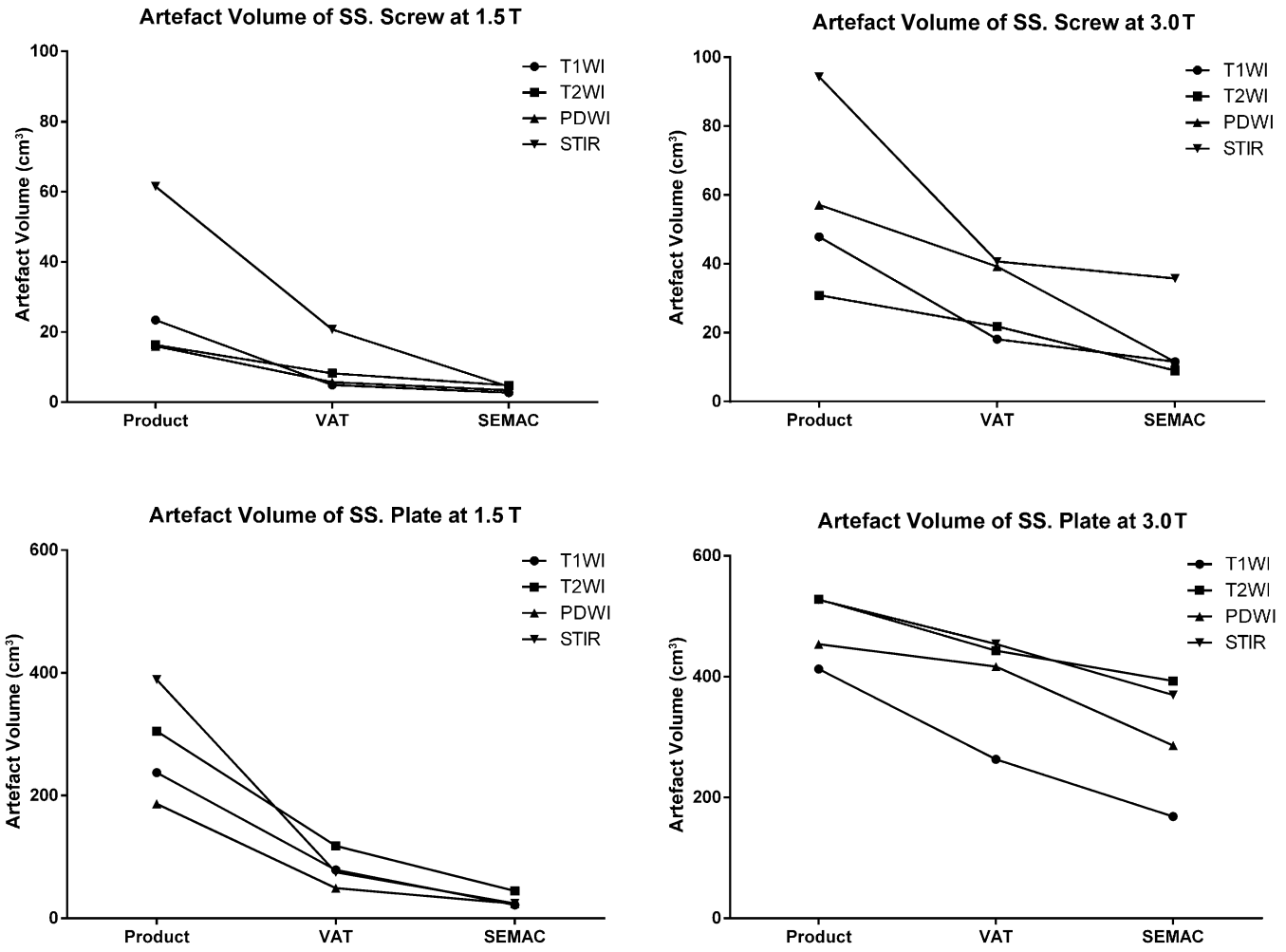

This study demonstrated that VAT and SEMAC-VAT, previously utilized at 1.5 T,[16] can be adapted to 3.0 T with similar success. Farrelly et al[20] found, in a phantom model, reductions in artefact severity with longer readout bandwidths with better overall image quality at 3.0 T. In addition to bandwidth considerations, previous work on improving MRI around metal implants has also focused on VAT techniques originally described by Cho et al.[13] Kolind et al[21] also described a VAT SE sequence utilizing high RF and readout bandwidths. This sequence was referred to as a "metal artefact reduction sequence". However, these studies only addressed in-plane distortion correction and did not deal with the topic of through-plane distortions. In contrast to VAT, SEMAC reduces through-plane distortions by utilizing additional phase-encoding steps for each excited slice. Implementation of the SEMAC technique requires only installation of appropriate software updates on existing whole-body MRI systems and does not depend upon any additional hardware installation.[14,22] However, as the performance of this sequence technique requires additional phase-encoding steps, SEMAC does increase scan time, which is a major drawback limiting its use in clinical routine.

Although the efficacy of SEMAC-VAT for the MRI of metal hardware has been shown at 1.5 T and recently at 3.0 T,[23] no study to date has made the comparison of the efficacy for this sequence technique between two commonly used field strengths (1.5 *vs* 3.0 T). In this evaluation, SEMAC-VAT demonstrated a similar amount of artefact reduction both at 1.5 and 3.0 T, when compared with conventional acquisitions. For successful correction of through-plane distortion, SEMAC-VAT requires a certain number of z-phase-encoding steps, depending upon the actual degree of distortion. Since scan time linearly increases with the applied number of phase-encoding steps ("*z*"), values beyond 15 may easily exceed a scan duration that is acceptable for routine examinations. In this study, we used 15 z-phase-encoding steps, which show effective artefact correction with an acquisition time of 8:41 (min:s) for 1.5 T and 12:32 (min:s) at 3.0 T for T_1 scans. Our study demonstrated that both SEMAC-VAT

Figure 5. Tissue specimen containing one plate and six stainless steel screws evaluated at 1.5 T (a, b) and 3.0 T (c, d), with proton density-weighted conventional sequence (a, c) and slice encoding for metal artefact correction with view angle tilting (SEMAC-VAT) technique (b, d). At both field strengths a substantial reduction in metal artefact was provided by SEMAC-VAT, allowing for better visualization of the tissue structures adjacent to the metal implants.

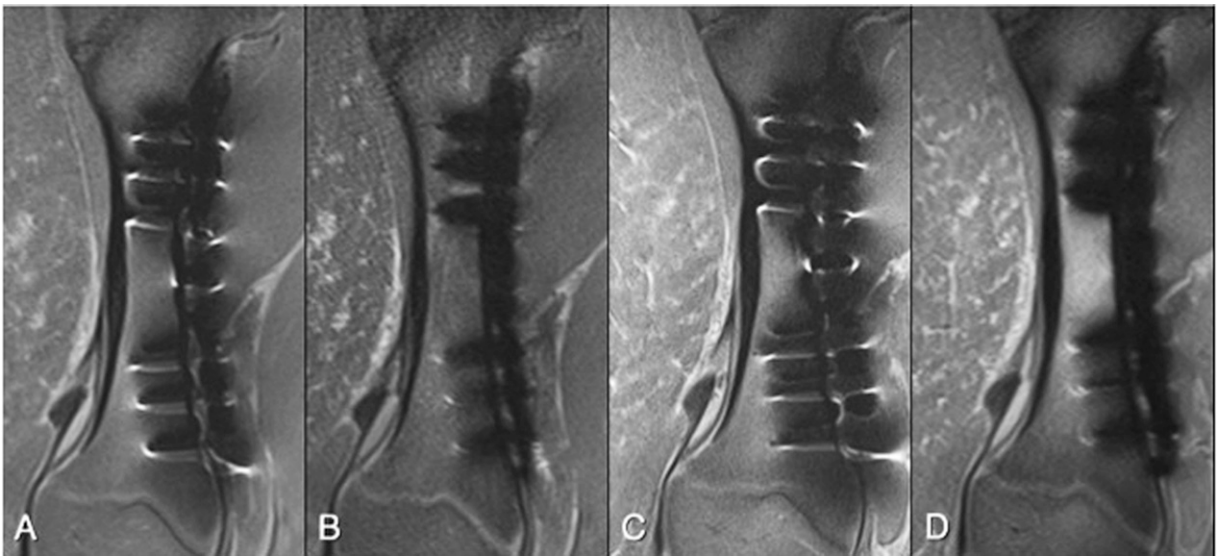

and VAT techniques reliably corrected for metal artefacts at both field strengths, based on T_1, T_2, PD and STIR images. Of all image contrasts, STIR sequences demonstrated the least degree of artefact reduction with SEMAC-VAT. The mechanism for disparities in artefact reduction based on image contrast remains unclear. It is possible that the semi-quantitative methodology employed for artefact volume measurements could be susceptible to thresholding effects. Thus, this method of volumetric artefact calculation may only be useful in comparing scans with identical image contrasts at the same field strength. However, in that context the method is a useful way to determine the efficacy of artefact reduction among the SEMAC-VAT and VAT sequences. The results regarding the STIR sequence also differ from those obtained by Sutter et al[9] in patients with total hip arthroplasty. In that study, only STIR and T_1 images were acquired. While both STIR and T_1 images with SEMAC-VAT resulted in improved image quality, SEMAC-VAT only improved diagnostic accuracy with the STIR images.

Scan time can be considerably reduced by utilizing dedicated acquisition techniques such as parallel imaging, partial Fourier sampling and long echo trains. A high RF pulse bandwidth is desired to limit the extent of slice distortion. However, an increase in RF pulse bandwidth increases the SAR, a critical limitation at 3.0 T. The increases in SAR resulted in prolonged acquisition times at 3.0 T. Because of the rising SAR, we got increasing measurement times at 3.0 T. Blurring may be observed on VAT sequences owing to the shear effect of the slice and a low-pass filter effect in the frequency domain during signal readout. Butts et al[24] reduced VAT-associated blurring by shortening the readout time. Generally, the readout time should not exceed the main lobe of the RF pulse's duration. This approach was implemented in the work herein. Of note, the shear effect blurs voxels in structures perpendicular to the slice, and the blur may be less if the structure is obliquely oriented relative to the slice. Higher readout bandwidth or a reduction in the number of readout samples can be used to shorten the readout time at the expense of lower SNR. The results in the present work demonstrated that high readout bandwidth (930 Hz per pixel) reduced image blurring with the SEMAC-VAT technique *vs* VAT. Only slight blurring could be recognized on the SEMAC-VAT images.

This study had several limitations. First, the method of volumetric measurements is limited, not only owing to the potential for thresholding effects described above but also owing to the fact that it represents a semi-quantitative measure requiring a user to perform histogram analyses. Nevertheless, the ease of use and of obtaining three-dimensional artefact measurements is advantageous. Second, the readers were blinded to the field strength at which the images were obtained. However, qualitative differences in the acquired images may have allowed the observers to discern the images that were obtained at 1.5 and at 3.0 T. This is a potential source of bias. The volumetric measurements of artefact reduction also differed considerably between field strengths. The reduction in relative artefact volume at 3.0 T (63%) was considerably greater than at 1.5 T (21%). As the SEMAC technique corrects through-plane distortions, and as these are generally much greater at 3.0 T, the artefact volume reduction may as a result be much more pronounced when SEMAC is applied. However, careful further study of these techniques at both field strengths would be useful to confirm this effect. Third, only three volunteer scans were performed. In the future, further *in vivo* studies of patients with metal implants will be required to obtain more conclusive information with regard to the clinical utility of these techniques. Finally, the current long acquisition times at 1.5 and 3.0 T for SEMAC-VAT sequences make it difficult to implement these sequences in routine clinical imaging. However, the results in this study have demonstrated that 15 z-phase-encoding steps allowed for

Table 5. The scoring of qualitative evaluation by readers with the calculation of intraclass correlation coefficient (ICC) for all study data

Imaging evaluation	1.5 T product			1.5 T SEMAC-VAT			3 T product			3 T SEMAC-VAT		
	Rater 1	Rater 2	Rater 3	Rater 1	Rater 2	Rater 3	Rater 1	Rater 2	Rater 3	Rater 1	Rater 2	Rater 3
Artefact size												
Mean	2.50	3.25	3.25	1.00	1.00	1.25	4.00	3.75	3.75	2.50	2.00	1.75
SD	0.50	0.43	0.43	0	0	0.43	0	0.43	0.43	0.50	0	0.43
ICC (95% CI)	0.95 (0.89–0.98)											
p-value	<0.001											
Structure distortion												
Mean	3.25	3.25	3.25	1.25	1.00	1.25	3.75	3.75	3.75	1.75	2.00	1.75
SD	0.43	0.43	0.43	0.43	0	0.43	0.43	0.43	0.43	0.43	0	0.43
ICC (95% CI)	0.99 (0.97–1.00)											
p-value	<0.001											
Imaging blur												
Mean	3.00	2.00	2.00	3.75	3.50	4.00	1.00	1.00	1.25	2.25	3.50	2.75
SD	0.71	0	0.71	0.43	0.50	0	0	0	0.43	0.43	0.50	0.43
ICC (95% CI)	0.88 (0.73–0.96)											
p-value	<0.001											
Visualization ability												
Mean	2.50	3.25	3.75	1.25	1.00	1.25	3.75	3.75	3.25	2.50	2.00	1.75
SD	0.87	0.43	0.43	0.43	0	0.43	0.43	0.43	0.43	0.87	0	0.43
ICC (95% CI)	0.91 (0.79–0.97)											
p-value	<0.001											
Overall image quality												
Mean	2.50	3.75	4.00	1.25	1.00	2.00	3.75	3.75	3.00	2.50	2.00	1.00
SD	0.87	0.43	0	0.43	0	0	0.43	0.43	0	0.87	0	0
ICC (95% CI)	0.80 (0.53–0.92)											
p-value	<0.001											

CI, confidence interval; product, conventional sequence; SD, standard deviation; SEMAC, slice encoding for metal artefact correction; VAT, view angle tilting.

Figure 6. A patient with stainless steel plate and six stainless steel screws placed for a Weber C fracture was imaged at 1.5 T (a, b) and 3.0 T (c, d) using short tau inversion recovery conventional sequence (a, c) and slice encoding for metal artefact correction with view angle tilting (SEMAC-VAT) technique (b, d). At both field strengths, a substantial reduction in metal artefact was achieved with SEMAC-VAT, on which the assessment of periprosthetic structures becomes possible. As noted, however, the image quality with SEMAC-VAT at 3.0 T seems better than at 1.5 T owing to higher signal-to-noise ratio, even though the artefact size is larger at 3.0 T.

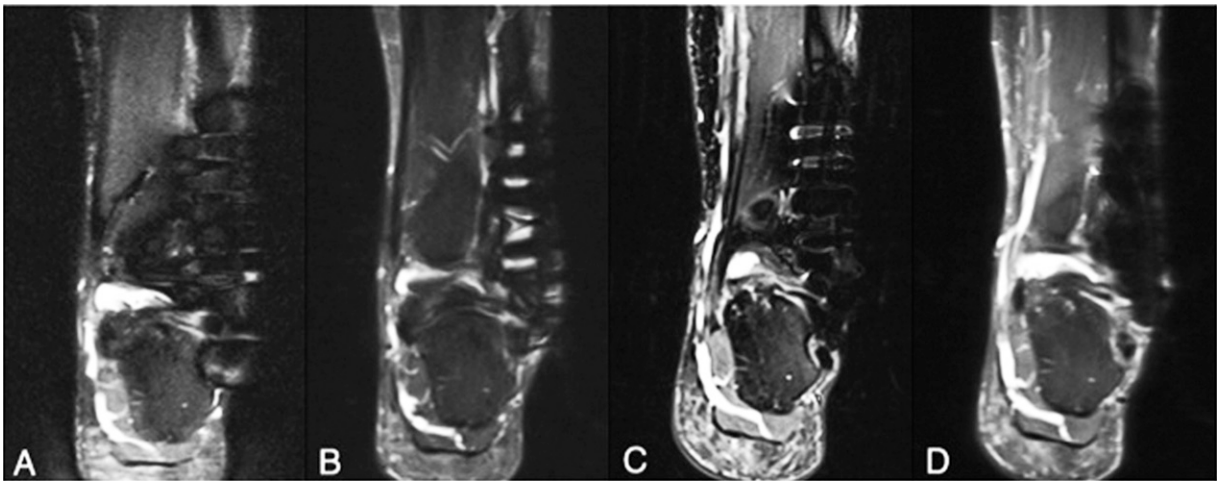

adequate artefact reduction for stainless steel prostheses, the type of metal implants that are supposed to cause the greatest susceptibility artefacts in MRI. In an ongoing project, we are trying to optimize the number of z-phase-encoding steps for individual patients with different types of metal implants, by using a distortion scout acquisition. This strategy will further shorten the scan time, making SEMAC-VAT technique more flexible and acceptable in the clinical setting.

In summary, SEMAC-VAT provides substantial reduction of metal-induced artefacts, a historical limitation to clinical MRI, in particular at 3.0 T. The use of SEMAC-VAT reduces susceptibility artefacts to a level less than that observed in sequences performed without such corrections at 1.5 T, markedly improving soft-tissue visualization adjacent to orthopaedic hardware at 3.0 T. This valuable imaging technique may help the radiologist in diagnosing recurrent tumour, fracture and infection in the region of implant or loosening of the implant. Whether applied at 1.5 or 3.0 T, SEMAC-VAT demonstrated a consistent reduction in the extent of metal artefacts.

FUNDING

This research was supported by grant from the National Natural Scientific Foundation of China (No. 81401388).

REFERENCES

1. Garvin KL, Konigsberg BS. Infection following total knee arthroplasty: prevention and management. *Instr Course Lect* 2012; **61**: 411–19.
2. Seil R, Pape D. Causes of failure and etiology of painful primary total knee arthroplasty. *Knee Surg Sports Traumatol Arthrosc* 2011; **19**: 1418–32. doi: 10.1007/s00167-011-1631-9
3. Kamishima T, Kitamura N, Amemiya M, Ishizaka K, Kato F, Yasuda K, et al. Experimental MR imaging of zirconia ceramic joint implants at 1.5 and 3 T. *Clin Radiol* 2010; **65**: 387–90. doi: 10.1016/j.crad.2009.12.007
4. Heyse TJ, Chong le R, Davis J, Boettner F, Haas SB, Potter HG. MRI analysis of the component-bone interface after TKA. *Knee* 2012; **19**: 290–4. doi: 10.1016/j.knee.2011.05.011
5. Hofmann S, Seitlinger G, Djahani O, Pietsch M. The painful knee after TKA: a diagnostic algorithm for failure analysis. *Knee Surg Sports Traumatol Arthrosc* 2011; **19**: 1442–52. doi: 10.1007/s00167-011-1634-6
6. Koch KM, Hargreaves BA, Pauly KB, Chen W, Gold GE, King KF. Magnetic resonance imaging near metal implants. *J Magn Reson Imaging* 2010; **32**: 773–87. doi: 10.1002/jmri.22313
7. Port JD, Pomper MG. Quantification and minimization of magnetic susceptibility artifacts on GRE images. *J Comput Assist Tomogr* 2000; **24**: 958–64.
8. Blankenstein FH, Truong B, Thomas A, Boeckler A, Peroz I. Influence on flux density of intraoral dental magnets during 1.5 and 3.0 tesla MRI. [In German.] *Rofo* 2011; **183**: 727–34. doi: 10.1055/s-0031-1273424
9. Sutter R, Ulbrich EJ, Jellus V, Nittka M, Pfirrmann CW. Reduction of metal artifacts in patients with total hip arthroplasty with slice-encoding metal artifact correction and view-angle tilting MR imaging. *Radiology* 2012; **265**: 204–14.
10. Ai T, Padua A, Goerner F, Nittka M, Gugala Z, Jadhav S, et al. SEMAC-VAT and MSVAT-SPACE sequence strategies for metal artifact reduction in 1.5T magnetic resonance imaging. *Invest Radiol* 2012; **47**: 267–76. doi: 10.1097/RLI.0b013e318240a919
11. Hayter CL, Koff MF, Shah P, Koch KM, Miller TT, Potter HG. MRI after arthroplasty: comparison of MAVRIC and conventional fast spin-echo techniques. *AJR Am J Roentgenol* 2011; **197**: W405–11. doi: 10.2214/AJR.11.6659
12. Chen CA, Chen W, Goodman SB, Hargreaves BA, Koch KM, Lu W, et al. New MR imaging methods for metallic implants in the knee: artifact

correction and clinical impact. *J Magn Reson Imaging* 2011; **33**: 1121–7. doi: 10.1002/jmri.22534
13. Cho ZH, Kim DJ, Kim YK. Total inhomogeneity correction including chemical shifts and susceptibility by view angle tilting. *Med Phys* 1988; **15**: 7–11.
14. Lu W, Pauly KB, Gold GE, Pauly JM, Hargreaves BA. SEMAC: slice encoding for metal artifact correction in MRI. *Magn Reson Med* 2009; **62**: 66–76. doi: 10.1002/mrm.21967
15. Koch KM, Brau AC, Chen W, Gold GE, Hargreaves BA, Koff M, et al. Imaging near metal with a MAVRIC-SEMAC hybrid. *Magn Reson Med* 2011; **65**: 71–82. doi: 10.1002/mrm.22523
16. Lee MJ, Janzen DL, Munk PL, MacKay A, Xiang QS, McGowen A. Quantitative assessment of an MR technique for reducing metal artifact: application to spin-echo imaging in a phantom. *Skeletal Radiol* 2001; **30**: 398–401.
17. Lee MJ, Kim S, Lee SA, Song HT, Huh YM, Kim DH, et al. Overcoming artifacts from metallic orthopedic implants at high-field-strength MR imaging and multi-detector CT. *Radiographics* 2007; **27**: 791–803.
18. Johnston C, Kerr J, Ford S, O'Byrne J, Eustace S. MRI as a problem-solving tool in unexplained failed total hip replacement following conventional assessment. *Skeletal Radiol* 2007; **36**: 955–61.
19. White LM, Kim JK, Mehta M, Merchant N, Schweitzer ME, Morrison WB, et al. Complications of total hip arthroplasty: MR imaging-initial experience. *Radiology* 2000; **215**: 254–62.
20. Farrelly C, Davarpanah A, Brennan SA, Sampson M, Eustace SJ. Imaging of soft tissues adjacent to orthopedic hardware: comparison of 3-T and 1.5-T MRI. *AJR Am J Roentgenol* 2010; **194**: W60–4. doi: 10.2214/AJR.08.1740
21. Kolind SH, MacKay AL, Munk PL, Xiang QS. Quantitative evaluation of metal artifact reduction techniques. *J Magn Reson Imaging* 2004; **20**: 487–95.
22. Lu W, Pauly KB, Gold GE, Pauly JM, Hargreaves BA. Slice encoding for metal artifact correction with noise reduction. *Magn Reson Med* 2011; **65**: 1352–7. doi: 10.1002/mrm.22796
23. Lee YH, Lim D, Kim E, Kim S, Song HT, Suh JS. Usefulness of slice encoding for metal artifact correction (SEMAC) for reducing metallic artifacts in 3-T MRI. *Magn Reson Imaging* 2013; **31**: 703–6. doi: 10.1016/j.mri.2012.11.004
24. Butts K, Pauly JM, Gold GE. Reduction of blurring in view angle tilting MRI. *Magn Reson Med* 2005; **53**: 418–24.